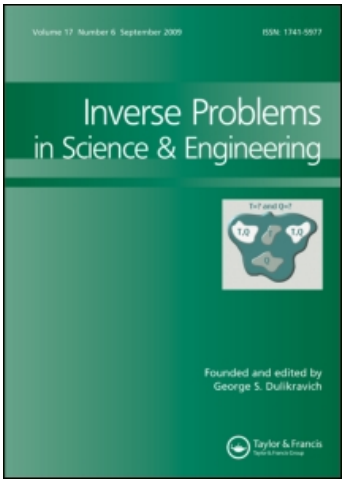

Inverse Problems in Science and Engineering
Publication details, including instructions for authors and subscription information:
http://www.informaworld.com/smpp/title~content=t713643452

An inverse problem for Helmholtz equation

M. Tadi[a]; A. K. Nandakumaran[b]; S. S. Sritharan[c]
[a] Department of Mechanical Engineering, University of Colorado Denver, Denver, CO 80217-3364, USA [b] Department of Mathematics, Indian Institute of Sciences, Bangalore, India [c] College of Science and Engineering, Naval Post-Graduate School, Monterey, CA 93943, USA

First published on: 30 March 2011

To cite this Article Tadi, M. , Nandakumaran, A. K. and Sritharan, S. S.(2011) 'An inverse problem for Helmholtz equation', Inverse Problems in Science and Engineering,, First published on: 30 March 2011 (iFirst)
To link to this Article: DOI: 10.1080/17415977.2011.556705
URL: http://dx.doi.org/10.1080/17415977.2011.556705

Inverse Problems in Science and Engineering
2011, 1–16, iFirst

Taylor & Francis
Taylor & Francis Group

An inverse problem for Helmholtz equation

M. Tadi[a]*, A.K. Nandakumaran[b] and S.S. Sritharan[c]

[a]*Department of Mechanical Engineering, University of Colorado Denver, Campus Box 112, P.O. Box 173364, Denver, CO 80217-3364, USA;* [b]*Department of Mathematics, Indian Institute of Sciences, Bangalore, India;* [c]*College of Science and Engineering, Naval Post-Graduate School, Monterey, CA 93943, USA*

(*Final version received 1 December 2010*)

This article is concerned with subsurface material identification for the 2-D Helmholtz equation. The algorithm is iterative in nature. It assumes an initial guess for the unknown function and obtains corrections to the guessed value. It linearizes the otherwise nonlinear problem around the *background field*. The background field is the field variable generated using the guessed value of the unknown function at each iteration. Numerical results indicate that the algorithm can recover a close estimate of the unknown function based on the measurements collected at the boundary.

Keywords: inverse problem; Helmholtz equation; elliptic system

AMS Subject Classifications: 31A25; 65N21

1. Introduction

In this article, we consider an inverse reconstruction algorithm for the Helmholtz equation. This problem appears very naturally in various applications including biomedical imaging [1,2], impedance imaging [3], optical imaging for non-destructive evaluation [4], and wave propagation and scattering [5]. It is instructive to discuss one example. Consider the propagation of the electromagnetic waves through the atmosphere. Writing Maxwell's equation in terms of the electric field, $\mathbf{E}(\mathbf{x})$, leads to the following vector wave equation [6]:

$$\nabla^2\mathbf{E} + \nabla[\mathbf{E}.\nabla(\log(\epsilon))] = \mu\frac{\partial^2(\epsilon\mathbf{E})}{\partial t^2}, \tag{1}$$

where μ is the permeability and $\epsilon(\mathbf{x})$ is the dielectric constant. Assuming a periodic incident wave, $\mathbf{E}(t,\mathbf{x}) = \mathbf{p}(\mathbf{x})\cos(\omega t)$, one arrives at

$$\nabla^2\mathbf{p} + \omega^2\mu\epsilon\mathbf{p} = -\nabla[\mathbf{p}.\nabla(\log(\epsilon))], \tag{2}$$

for the amplitude of the electric field, $\mathbf{p}(\mathbf{x})$. The dielectric constant $\epsilon(\mathbf{x})$ is a function of the domain and, in general, is not known. It can also be argued that, for a wide range of applications, the right-hand side in the above equation can be neglected in comparison to

*Corresponding author. Email: mohsen.tadi@ucdenver.edu

ISSN 1741–5977 print/ISSN 1741–5985 online

DOI: 10.1080/17415977.2011.556705
http://www.informaworld.com

the other two terms [6, p. 232]. It is then clear that, in order to recover the dielectric constant, one is led to deal with the Helmholtz equation.

For an elliptic system, there are two classes of problems that are often referred to as *inverse* problems. One class of problems considers the case in which part of the boundary is not accessible and no boundary data are available. The interest is then to recover the unknown boundary conditions based on measurements collected at the part of the boundary that is accessible [7–9]. In the other class of problems, which is the topic of this work, the interest is in identifying a subsurface material property based on the measurements collected at the boundary. It is well-known that both classes of problems are highly *ill-posed* [10] and various methods have been developed to overcome it.

A number of methods have been developed for the specific inverse problem considered here. These efforts include Newton based methods [11,12], layer stripping methods [13,14], point-source method [15,16], factorization method [17], continuation method [18] and level set method [19]. The purpose of this article is to apply a recently developed method, [20,21], to the problem of subsurface evaluation for the Helmholtz equation. The method is quite versatile and can be applied to various system. It has been developed and applied to parabolic systems due to their severe ill-posedness. Section 2 presents the algorithm and Section 3 uses two numerical examples to show the applicability of the method.

2. Helmholtz equation and inversion

Let $S \subset R^2$ be a closed bounded set. Consider a 2-D Helmholtz equation given by

$$\Delta u + k^2 g(\mathbf{x}) u = 0, \quad \mathbf{x} \in S \subset R^2, \tag{3}$$

where Dirichlet boundary conditions are given at the boundary of S, denoted by ∂S.

$$u(\mathbf{x}) = \tau(\mathbf{x}), \quad \mathbf{x} \in \partial S. \tag{4}$$

The variable $u(\mathbf{x})$ denotes the electric field, the parameter k denotes the frequency of the incident wave and the function $g(\mathbf{x})$ is a physical parameter. The goal is to recover the function $g(\mathbf{x})$ based on boundary measurements. For our application, the permeability of the domain, μ, is equal to one, and $g(\mathbf{x}) = \epsilon(\mathbf{x})$ in Equation (2). A similar equation appears in applications in time-harmonic acoustic wave [22] where $g(\mathbf{x})$ is related to the refractive index of the domain. Also, the above equation appears in optical tomography imaging [23]. Assume that on parts of the boundary, in addition to the given Dirichlet condition, data can be collected in the form of the Neumann condition given by

$$\frac{\partial u}{\partial n}(\mathbf{x}) = \eta(\mathbf{x}), \quad \mathbf{x} \in \partial S, \tag{5}$$

where $\frac{\partial u}{\partial n}$ is the normal derivative. The inverse problem is now to recover the unknown function, $g(\mathbf{x})$, based on the collected data at the boundary. The method can be applied to 3-D domains, however for simplicity, we consider a square region in 2-D. The present algorithm is iterative in nature and it consists of the following steps.

I. Assume an initial guess: It is often the case that the goal is to recover an interior abnormality within an otherwise uniform material property. It is then reasonable to assume a uniform guess for the unknown function given by $\hat{g}(\mathbf{x})$. The initial guess together with the given Dirichlet boundary conditions leads to a background field, $\hat{u}(\mathbf{x})$,

which satisfies the forward problem given by

$$\Delta\hat{u} + k^2\hat{g}(\mathbf{x})\hat{u} = 0, \quad \mathbf{x} \in S, \quad \hat{u}(\mathbf{x}) = \tau(\mathbf{x}), \quad \mathbf{x} \in \partial S. \tag{6}$$

This field satisfies the Dirichlet conditions at all four sides. Since the initial guess is almost always not the actual function, the computed field is not the actual field. Let $e(\mathbf{x})$ denote the error, i.e. $e(\mathbf{x}) = u(\mathbf{x}) - \hat{u}(\mathbf{x})$, and subtract the two equations to obtain an equation for the error given by

$$\Delta e + k^2 g(\mathbf{x})u - k^2\hat{g}(\mathbf{x})\hat{u} = 0, \quad \mathbf{x} \in S, \quad e(\mathbf{x}) = 0, \quad \mathbf{x} \in \partial S. \tag{7}$$

It is also possible to write $g(\mathbf{x}) = \hat{g} + h$ where $h(\mathbf{x})$ is unknown. It follows that

$$\Delta e + k^2\hat{g}e + k^2 h(\mathbf{x})u(\mathbf{x}) = 0, \quad \mathbf{x} \in S, \quad e(\mathbf{x}) = 0, \quad \mathbf{x} \in \partial S. \tag{8}$$

Here, there is one equation and two unknowns, namely $h(\mathbf{x})$ and $u(\mathbf{x})$ ($e(\mathbf{x})$ is also unknown, but is related to $u(\mathbf{x})$). It is possible to linearize around the background field and arrive at,

$$\Delta e + k^2\hat{g}e + k^2 h(\mathbf{x})\hat{u} = 0, \quad \mathbf{x} \in S, \quad e(\mathbf{x}) = 0, \quad \mathbf{x} \in \partial S. \tag{9}$$

Now, there are still two unknowns. However, the function $e(\mathbf{x})$ is required to satisfy two boundary conditions on the side at which the data are collected. It is possible to consider two separate problems.

II. Consider two different problems for $e(\mathbf{x})$: The two well-posed elliptic problems for $e(\mathbf{x})$ are given by

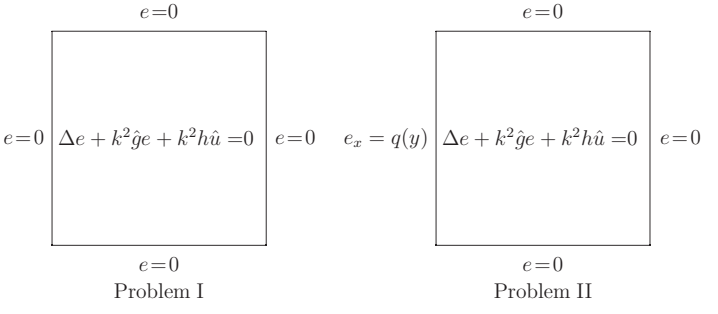

Figure 1. Two elliptic problems for the error field.

where $q(y) = u_x(0, y) - \hat{u}_x(0, y)$. Note that $u_x(0, y)$ is the collected data, and $\hat{u}_x(0, y)$ can be computed from the background field.

The same symbol, $e(\mathbf{x})$, is being used here to denote the error in both of these problems. In what follows, it will specifically be clear which problem is being considered. After finite-dimensional discretization, these two equations lead to

$$\mathbf{A}_0\bar{e} + k^2\bar{h}(\mathbf{x})\bar{u}(\mathbf{x}) = 0, \quad \text{Problem I} \tag{10}$$

and

$$\mathbf{A}_1\bar{e} + k^2\bar{h}(\mathbf{x})\bar{u}(\mathbf{x}) = \bar{q}, \quad \text{Problem II.} \tag{11}$$

The quantities $\bar{e}, \bar{h}, \bar{u}$ and $\bar{q}$ are finite-dimensional representations of the variables e, h, $\hat{u}$ and $\tilde{q}$. The matrices $\mathbf{A}_0$ and $\mathbf{A}_1$, and the vector $\bar{u}$ are known. Also, the condition $e_x = q(y)$ appears in the vector $\bar{q}$ in Equation (11).

The error, $\bar{e}$, is still unknown and so is $\bar{h}$. But now, there are two equations and two unknowns. One can obtain one equation for $\bar{h}$ by eliminating the $\bar{e}$. It follows that

$$k^2(\mathbf{A}_0^{-1} - \mathbf{A}_1^{-1})\bar{u}\bar{h} = -\mathbf{A}_1^{-1}\bar{q}. \tag{12}$$

The above equation can now be solved for $\bar{h}(\mathbf{x})$. The collected data show up in the vector $\bar{q}$ on the right-hand side of Equation (12). As it is expected, the coefficient matrix is singular. However, one can solve for the unknown vector with the help of Tikhonov regularization. One can introduce Tikhonov regularization by considering the over-determined linear system given by

$$\begin{bmatrix} k^2(\mathbf{A}_0^{-1} - \mathbf{A}_1^{-1})\bar{u} \\ \beta\Phi \\ \beta\Theta \end{bmatrix} \bar{h} = \begin{bmatrix} -\mathbf{A}_1^{-1}\bar{q} \\ 0 \\ 0 \end{bmatrix}, \tag{13}$$

where β is a pre-specified positive constant, and Φ and Θ are matrix representations of the first-order derivatives in x and y. The above over-determined system can now be solved for $\bar{h}$ using least-square method.

III. Update the assumed value: With $\bar{h}$ computed, one can update the assumed value of the unknown function according to

$$\hat{g}(\mathbf{x}) = \hat{g}(\mathbf{x}) + h(\mathbf{x}), \tag{14}$$

and proceed to step I.

The error shows up in the vector $\bar{q}$. As the iterations proceed, the value of the error is reduced.

3. Specific approximations and numerical results

In this section, we use a number of numerical examples to investigate the applicability of the proposed method. The above algorithm involves the numerical solution of the Helmholtz equation. It is well-known that, for high frequencies, the numerical solution of Helmholtz equation remains challenging [24,25]. It is also noted that the present algorithm requires the inverse of the matrices that appear in Equation (12). Therefore, although sparse solvers can be used to improve the accuracy of the forward problem in Equation (6), the need for the actual inverse of the matrices in Equation (12) dictates the range of the applicable system parameters. This is entirely a numerical issue. The goal of this article is to investigate the applicability of the present inversion method to the Helmholtz equation.

It is possible to obtain working equations by using the finite-difference method. The domain can be divided into 60 equal intervals in both x and y directions with $\Delta x = \Delta y = \frac{1}{60}$. Using central fourth-order and one-sided second-order accurate finite-difference schemes, it is possible to compute various terms in Equations (12) and (13). For this choice for the mesh, the dimension of the linear system in Equation (12) is 3721. Our numerical experiments indicated that this mesh size is adequate for the frequencies studied in this article. Little change in the solution of the forward problem was noticed.

We first consider recovering one interior target. The actual function $g(x, y)$ is given by $g(x, y) = 1 + \exp[-\frac{(0.3-x)^4}{0.0001}]\exp[-\frac{(0.3-y)^4}{0.0001}]$ and is shown in Figure 4. For simplicity, it is assumed that the domain is exposed to the external field given by $u(x, y) = \cos(k(x\cos(\theta) + y\sin(\theta)))$, where θ is the direction for the incoming wave. The necessary Dirichlet conditions are then given by

$$u(x, 0) = \cos(k(x\cos(\theta))), \quad u(x, 1) = \cos(k(x\cos(\theta) + \sin(\theta))), \tag{15}$$

$$u(0, y) = \cos(y\sin(\theta))), \quad u(1, y) = \cos(k(\cos(\theta) + y\sin(\theta))). \tag{16}$$

In practice, the boundary is accessible and it is possible to collect data on all sides of the domain. Here, we assume that measurements are collected at one side identified by $x = 0$ and $y \in [0, 1]$. The given measurements are the slope of the field on this side.

It is also possible to collect data for a number of frequencies and a number of incoming wave angles. Formulations for these different sets of experiments can be added to the least-square problem given in Equation (13) according to

$$\begin{bmatrix} \mathbf{G}(k_1, \theta_1) \\ \mathbf{G}(k_1, \theta_2) \\ \vdots \\ \mathbf{G}(k_2, \theta_1) \\ \mathbf{G}(k_2, \theta_2) \\ \vdots \\ \hline \beta\Phi \\ \beta\Theta \end{bmatrix} \bar{h} = \begin{bmatrix} -\mathbf{A}_1^{-1}\bar{q}_1^{(1)} \\ -\mathbf{A}_1^{-1}\bar{q}_2^{(1)} \\ \vdots \\ -\mathbf{A}_1^{-1}\bar{q}_1^{(2)} \\ -\mathbf{A}_1^{-1}\bar{q}_2^{(2)} \\ \vdots \\ \hline 0 \\ 0 \end{bmatrix}, \quad \text{or } \Gamma\bar{h} = \gamma, \tag{17}$$

where

$$\mathbf{G}(k_i, \theta_j) = (k_i^2(\mathbf{A}_0^{-1} - \mathbf{A}_1^{-1})\bar{u}). \tag{18}$$

In the above equation, each row corresponds to the collected data for the frequency k_i and the incident angle θ_j. On the right-hand side, the subscripts in $\bar{q}_i^{(j)}$ correspond to the frequency, and the superscripts correspond to the incident angle. In addition, for simplicity, Equation (17) also denotes the coefficient matrix by Γ and the right-hand side by γ. The least-square solution to the above over-determined system is given by

$$\bar{h} = [\Gamma^\top\Gamma]^{-1}\Gamma^\top\gamma. \tag{19}$$

Consider the above least-square problem before the inclusion of the Tikhonov regularization. In order to see the effect of including additional experimental data, it is instructive to look at the singular values of the coefficient matrix, Γ, or the eigenvalues of the symmetric non-negative matrix, $[\Gamma^\top\Gamma]$. Figure 2 shows the eigenvalues of the symmetric matrix $[\Gamma^\top\Gamma]$ for a single frequency $k = 10$. The eigenvalues are normalized with respect to their highest value and they are plotted as formulations for different values of the incident angles are added to the least-square problem. The figure shows that, when formulations for nine different incident angles are included, the coefficient matrix has the largest number of non-zero eigenvalues. Figure 3 suggests the same behaviour when formulations for three different frequencies are included, i.e. $k = 10$, 15, 17. The incident angle for these experiments is $\theta = \frac{\pi}{18}$.

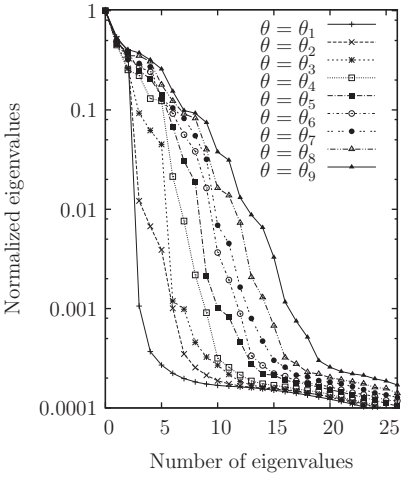

Figure 2. Normalized singular values of the coefficient matrix using the formulations for only one frequency $k = 10$.

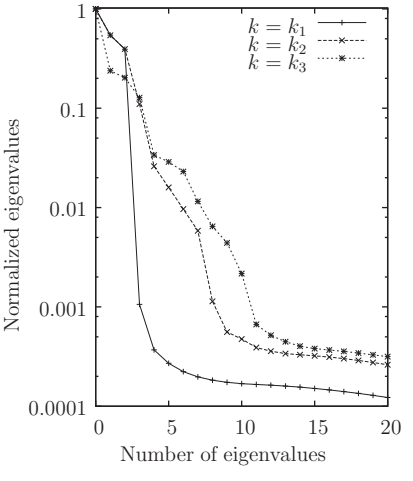

Figure 3. Normalized singular values of the coefficient matrix using the formulations for only one angle of incident $\theta = \frac{\pi}{18}$.

Example 1 It is now possible to proceed with the inversion algorithm and consider recovering the material property. The actual function is given by

$$g(x, y) = 1 + \exp\left[-\frac{(0.3 - x)^4}{0.0001}\right] \exp\left[-\frac{(0.3 - y)^4}{0.0001}\right], \tag{20}$$

and is shown in Figure 4. The data are collected for four different frequencies. For each frequency, nine different incident angles are considered. The four frequencies are given by

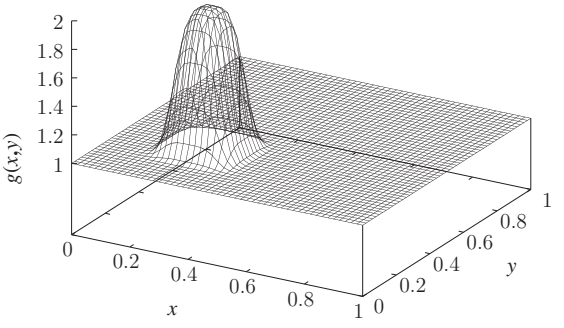

Figure 4. The unknown function to be recovered in Example 1.

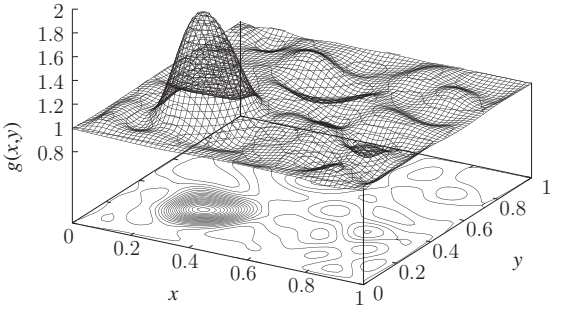

Figure 5. The recovered function with 8% signal-to-noise ratio.

$k_i = 10$, 15, 17, 19, and the nine angles are given by $\theta_j = \frac{\pi}{18}, \frac{\pi}{15}, \frac{\pi}{10}, \frac{\pi}{7}, \frac{\pi}{5}, \frac{\pi}{4}, \frac{\pi}{3.5}, \frac{\pi}{3}, \frac{\pi}{2.5}$. In order to model the noise in the data, the given data are contaminated with a zero-mean white noise with the noise-to-signal ratio of 8%.

It is easy to note that the dimension of the least-square problem can become exceedingly large, when all of the available data are used at the same time. In fact, the bulk of the computational burden is in computing the matrix multiplication in Equation (19). On the other hand, matrix–matrix calculation can be performed very efficiently on a parallel machine. In what follows, the data for nine different incident angles are used at the same time. However, the algorithm is repeated for each frequency.

For this study, we do not use any method to choose an optimal value for the parameter β. This parameter controls the amount of smoothness that is imposed in the least-square problem. We can start with a relatively large value for this parameter and monitor the error as the iterations proceed. As we reduce this parameter, the error reduces at a faster rate. There is also a minimum value for this parameter after which, if this parameter is reduced further, then numerical instability sets in and the iterations diverge. For all the examples in this article, there is a range for the value of β that can lead to successful inversion.

It is possible to start the algorithm from a uniform initial guess, i.e. $\hat{g}(x, y) = 1$ for the first frequency $k_1 = 10$. After a reasonable amount of reduction in error is achieved, it is then possible to use the collected data for the next frequency, i.e. $k_2 = 15$. The output from the first iteration, using $k = 10$, can be used as the initial guess for the second iteration, using $k = 15$. This process can be repeated for the remaining data. Figure 5 shows the recovered function which is in good agreement with the sought after function.

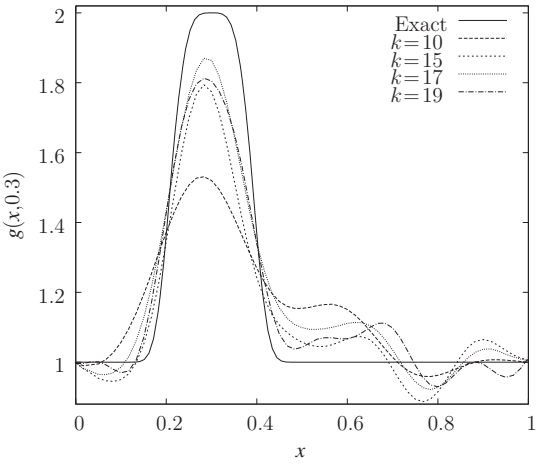

Figure 6. A cross-section of the recovered functions and their comparison to the actual function for Example 1. The functions are the outputs from the algorithm using the data for the indicated frequencies. The results are for a fixed value of $y=0.3$.

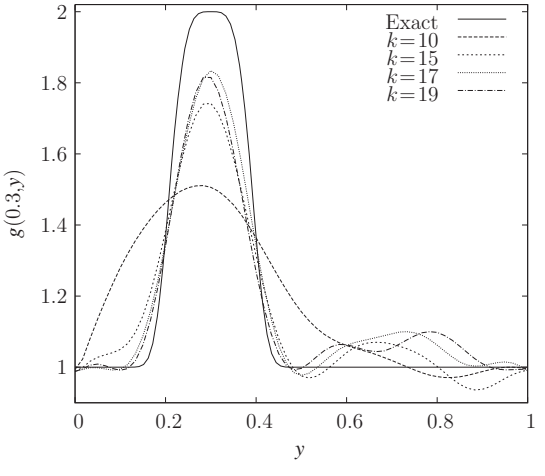

Figure 7. A cross-section of the recovered functions and their comparison to the actual function for Example 1. The functions are the outputs from the algorithm using the data for the indicated frequencies. The results are for a fixed value of $x=0.3$.

For each frequency the algorithm is allowed to iterate 35 times. Figures 6 and 7 show two cross-sections of the unknown function and compare them to the actual function. The indicated functions are the outputs for each frequency. The parameter β is set at $\beta=0.0005$.

It is also possible to monitor the error as the iterations proceed. For each iteration, it is possible to compute the error which is given by

$$\text{Error}=\sum_{\ell=1}^{61}\left[u_{x_\ell}-\hat{u}_{x_\ell}\right]^2,\quad \text{where } u_{x_\ell}=u_x(0,(\ell-1)\Delta y)\ \text{ and }\ \hat{u}_{x_\ell}=\hat{u}_x(0,(\ell-1)\Delta y). \tag{21}$$

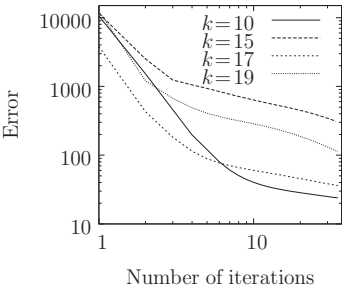

Figure 8. Reduction in the error for the four stages of the algorithm as functions of iterations for Example 1. The algorithm performs 35 iterations for each frequency.

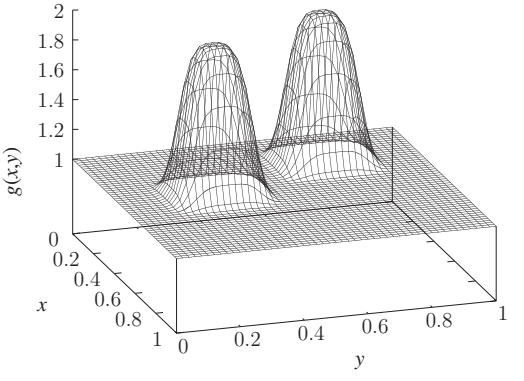

Figure 9. The unknown function with two interior targets to be recovered in Example 2.

Figure 8 shows the reduction in the error for the first example. The algorithm treats the data for each frequency separately.

Example 2 We next consider an example with two targets. Consider boundary evaluation of the function given by

$$g(x,y) = 1 + \exp\left[-\frac{(0.25-x)^4}{0.00015}\right]\exp\left[-\frac{(0.7-y)^4}{0.00015}\right] + \exp\left[-\frac{(0.45-x)^4}{0.00015}\right]\exp\left[-\frac{(0.3-y)^4}{0.00015}\right]. \tag{22}$$

The actual function is also shown in figure 9. Figure 10 shows the recovered function. For this case, the algorithm is allowed to iterate 50 times for each frequency. The parameter β is chosen as $\beta = 0.00035$. Figures 11 and 12 show two cross-sections of the computed function. The figures show the computed values after 50 iterations for each frequency and compare them to the actual values. One can note that the algorithm can recover a better estimate of the target that is closer to the boundary at which measurements are collected.

The algorithm exhibits a relatively good robustness to noise. For both examples, the signal-to-noise ratio is 8%. Figure 13 shows the recovered function for the second

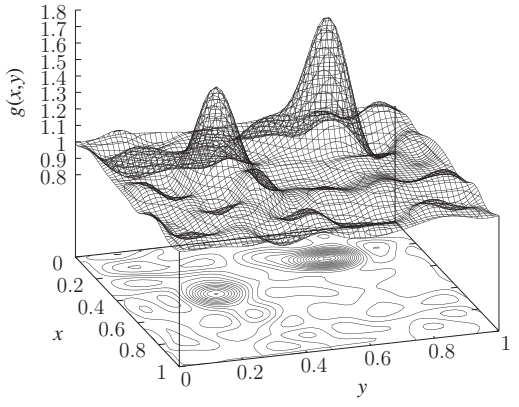

Figure 10. The recovered function with 8% signal-to-noise ratio for Example 2. The algorithm performs 50 iterations for each frequency.

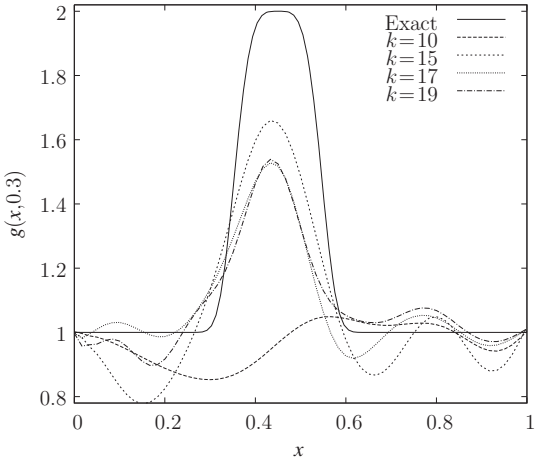

Figure 11. A cross-section of the recovered functions and their comparison to the actual function for Example 2. The functions are the outputs from the algorithm using the data for the indicated frequencies. The results are for a fixed value of $y = 0.3$.

example, if the level of noise is reduced to 4%. As expected, a relatively better estimate of the unknown function is obtained.

It is also possible to improve the results by using the recovered function, given in Figure 13, as the initial guess for the algorithm. The algorithm in the present form uses the data for the given four frequencies separately. Figure 14 shows the recovered function, when the given data are used twice. Figures 15 and 16 compare the exact solutions to the recovered functions at two different cross-sections.

Example 3 We next consider the same problem as in Example 2, and assume that the data are collected at two sides. In other words, in addition to the data at $x = 0$, i.e. $u_x(0, y)$,

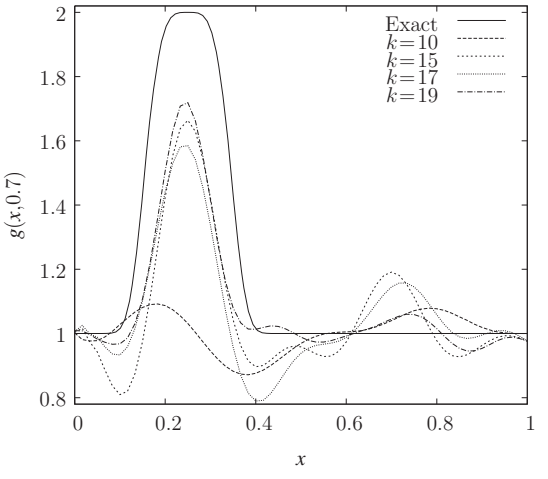

Figure 12. A cross-section of the recovered functions and their comparison to the actual function for Example 2. The functions are the outputs from the algorithm using the data for the indicated frequencies. The results are for a fixed value of $y = 0.7$.

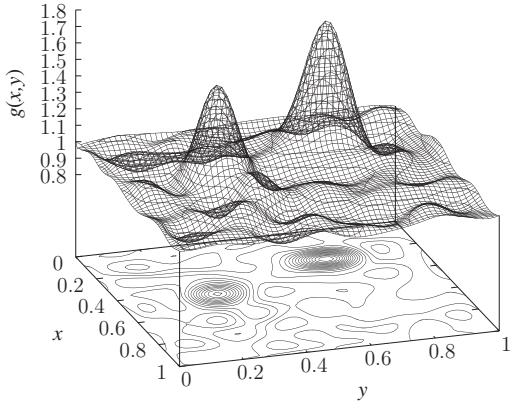

Figure 13. The recovered function with 4% signal-to-noise ratio for Example 2. The algorithm performs 50 iterations for each frequency.

we assume that the flux at the top surface can also be provided, i.e. $u_y(x, 1)$. The two problems that we consider for the error field are given in Figure 17, where the error in the flux at the top boundary is given by $\sigma(x) = u_y(x, 1) - \hat{u}_y(x, 1)$. For this case, we choose the noise-to-signal ratio as 0.04% and keep the same angles of incident and frequencies. Figure 18 shows the recovered function. Figures 19 and 20 show the recovered function at two cross-sections and compare them to the actual function. The results are somewhat better. The recovered function for the target that is close to the top boundary compares better with the actual function. The parameter β is chosen as $\beta = 0.00085$. Similar to Example 2, it is also possible to improve the results by using the recovered function as the initial guess for the algorithm and use the data again.

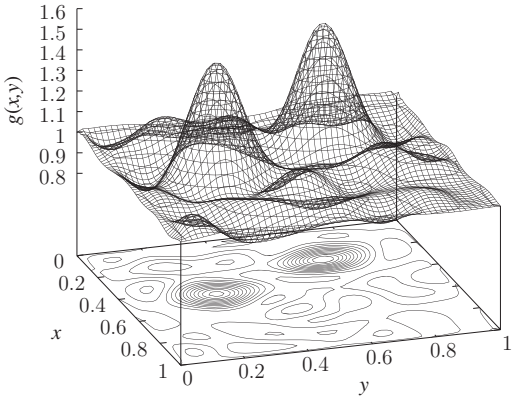

Figure 14. The recovered function for Example 2, when the recovered function given in Figure 13 is used as the initial guess.

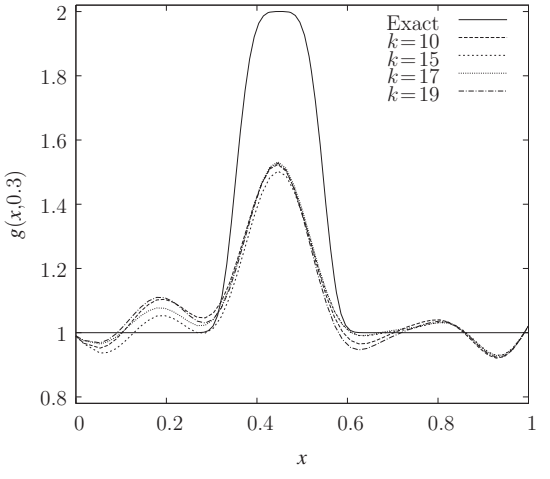

Figure 15. A cross-section of the recovered functions and their comparison to the actual function for Example 2, using the recovered function given in Figure 13 as the initial guess. The functions are the outputs from the algorithm using the data for the indicated frequencies. The results are for a fixed value of $y = 0.3$.

The results for the unknown function show little sensitivity to the angle of incident for the incoming wave, i.e. θ, as long as the chosen angles are such that they generate measurements that are linearly independent. In terms of the frequency of the incoming wave, our limitation is in terms of the accuracy of the forward problem. Results were less accurate for certain frequencies that are close to the eigenvalues of Helmholtz's operator. However, since we do not know the unknown function, therefore it is not possible to know these frequencies a prior.

Using the additional data in Example 3, it is possible to generate two forward problems. With two forward problems, it is possible to generate two equations for the

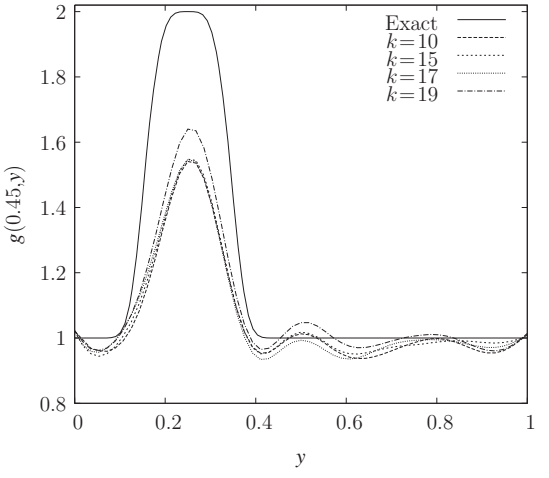

Figure 16. A cross-section of the recovered functions and their comparison to the actual function for Example 2, using the recovered function given in Figure 13 as the initial guess. The functions are the outputs from the algorithm using the data for the indicated frequencies. The results are for a fixed value of $x = 0.45$.

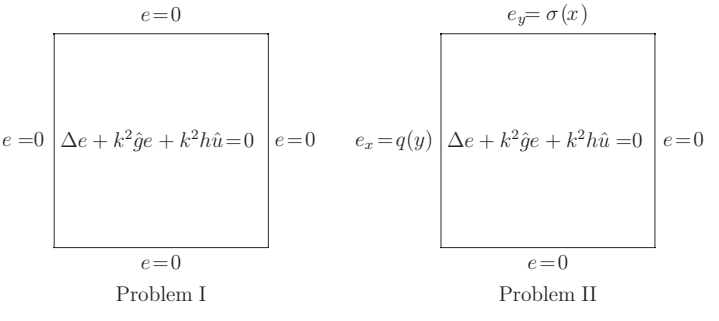

Figure 17. Two elliptic problems for the error field with additional measurements used in Example 3.

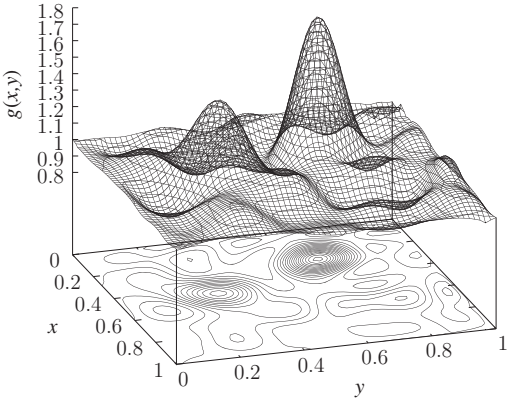

Figure 18. The recovered function with 4% signal-to-noise ration for Example 3.

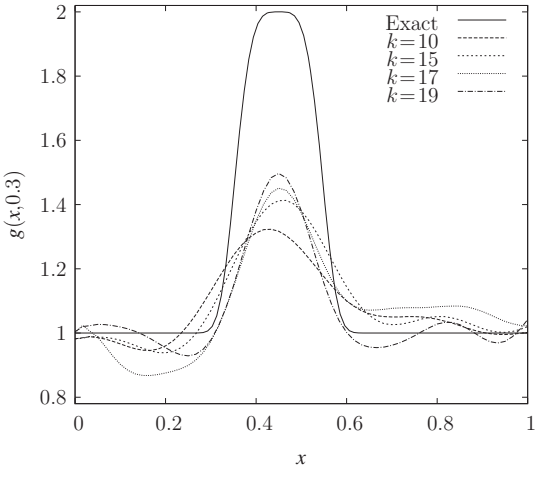

Figure 19. A cross-section of the recovered functions and their comparison to the actual function for Example 3. The functions are the outputs from the algorithm using the data for the indicated frequencies. The results are for a fixed value of $y=0.3$.

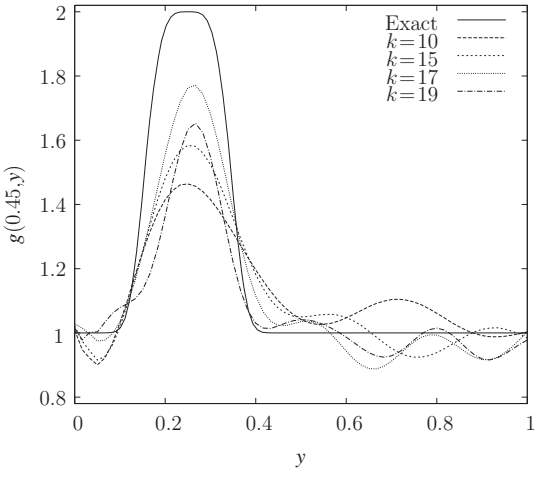

Figure 20. A cross-section of the recovered functions and their comparison to the actual function for Example 3. The functions are the outputs from the algorithm using the data for the indicated frequencies. The results are for a fixed value of $x=0.45$.

unknown function. Using two forward problems, we were able to improve the results significantly for an inverse parabolic problem [26]. Here, we are limited by the available computational resources. The algorithm can be improved in a number of ways, and they will explored in future works.

4. Conclusions

In this article, we studied the application of a new method to the subsurface material identification for the Helmholtz equation. The method shows good robustness to

the noise. Results can be improved by collecting measurements at additional locations on the boundary. The method is general and can, in principle, be applied to the Helmholtz equation with any incident frequency. The results presented here are for low-range frequencies. This is entirely a numerical issue. Numerical results can also be greatly improved by using a finer mesh and/or, more accurate finite-difference approximations. The targets in both examples include regions with very high gradients and smaller mesh sizes are indeed required for accurate calculation of the working equations. It is also possible to change the ordering in the algorithm. In other words, it is possible to include the formulations for the four frequencies in each iterations. The algorithm can then be repeated individually for each incident angle. All of these issues will be addressed in future works.

References

[1] National Research Council, *Mathematics and Physics of Emerging Biomedical Imaging*. National Academic Press, Washington DC, 1996.
[2] S.R. Arridge, *Optical tomography in medical imaging*, Inverse Probl. 15 (1999), pp. R41–R93.
[3] K. Bryan and T. Leise, *Impedance imaging, inverse problems, and Harry Potter's cloak*, SIAM Rev. 52(2) (2010), pp. 359–377.
[4] M. Born and E. Wolf, *Principles of Optics*, Pergamon, New York, 1964.
[5] G.M.L. Gladwell and N.B. Willms, *On the mode shapes of the Helmholtz equation*, J. Sound Vib. 188 (1995), pp. 419–433.
[6] J.W. Strohbehn (ed.), *Laser Beam Propagation in the Atmosphere*, Springer-Verlag, New York, 1978.
[7] B. Jin and Y. Zheng, *A meshless method for some inverse problems associated with the Helmholtz equation*, Comput. Methods Appl. Mech. Eng. 195 (2006), pp. 2270–2288.
[8] X.T. Xiong, *A regularization method for a Cauchy problem of the Helmholtz equation*, J. comput. Appl. Math. 233 (2010), pp. 1723–1732.
[9] H. Cao, M.V. Klibanov, and S.V. Pereverzev, *A Carleman estimate and the balancing principle in the quasi-reversibility method for solving the Cauchy problem for the Laplace equation*, Inverse Probl. 25(3) (2009), 035005 [21 pages].
[10] A.N. Tikhonov and V. Arsenin, *Solutions of Ill-posed Problems*, Wiley, New York, 1977.
[11] H.M. Varma, A.K. Nandakumaran, and R.M. Vasu, *Study of turbid media with light: Recovery of mechanical and optical properties from boundary measurement of intensity autocorrelation of light*, J. Opt. Soc. Am. A 26(4) (2009), pp. 1472–1483.
[12] H.M. Varma, B. Banerjee, D. Roy, A.K. Nandakumaran, and R.M. Vasu, *Convergence analysis of the Newton algorithm and a pseudo-time marching scheme for diffuse correlation tomography*, J. Opt. Soc. Am. A 27(2) (2010), pp. 259–267.
[13] J. Sylvester, D. Weinebrenner, and F. Gylys-Colwell, *Layer stripping for the Helmholtz equation*, SIAM J. Appl. Math. 56(3) (1996), pp. 736–754.
[14] Y. Chen, *Inverse scattering via skin effect*, Inverse Probl. 13 (1997), pp. 647–667.
[15] R. Potthast, *A fast new method to solve inverse scattering problems*, Inverse Probl. 12 (1996), pp. 731–742.
[16] M.F. Ben Hassen, K. Erhard, and R. Potthast, *The point-source method for 3D reconstructions for the Helmholtz and Maxwell equations*, Inverse Probl. 22 (2006), pp. 331–353.
[17] A. Kirsch and N. Grinberg, *The Factorization Method for Inverse Problems*, Oxford University, New York, 2008.
[18] G. Bao, S. Hou, and P. Li, *Inverse scattering by a continuation method with initial guesses from a direct imaging algorithm*, J. Comput. Phys. 227 (2007), pp. 755–762.

[19] O. Dorn, E. Miller, and C. Rappaport, *A shape reconstruction method for electromagnetic tomography using adjoint fields and level sets*, Inverse Probl. 16 (2000), pp. 1119–1156.
[20] M. Tadi, *An iterative method for the solution of ill-posed parabolic systems*, Appl. Math. Comput. 201(1–2) (2008), pp. 843–851.
[21] M. Tadi, *A computational method for an inverse problem in a parabolic systems*, Disc. Contin. Dyn. Syst.-B 12(1) (2009), pp. 205–218.
[22] Y.Y. Lu, *A fourth-order Magnus scheme for Helmholtz equation*, J. Comput. Appl. Math. 173 (2005), pp. 247–258.
[23] E. Scherleitner and B.G. Zagar, *Optical tomography imaging based on higher order born approximation of diffuse photon density waves*, IEEE Trans. Instrum. Meas. 54(4) (2005), pp. 1607–1611.
[24] M. Navabi, M.H. Kamran Siddiqui, and J. Daragahi, *A new 9-point sixth-order accurate compact finite difference method for the Helmholtz equation*, J. Sound Vib. 307 (2007), pp. 972–982.
[25] G. Sutmann, *Compact finite difference schemes of sixth order for the Helmholtz equation*, J. Comput. Appl. Math. 203 (2007), pp. 15–31.
[26] M. Tadi, *Solution of an ill-posed parabolic equations based on multiple background field*, Adv. Math. Sci. J. 1 (2009), pp. 1–20.